JCTC Journal of Chemical Theory and Computation

Article

pubs.acs.org/JCTC

Martini Force Field Parameters for Glycolipids

César A. López,[†] Zofie Sovova,[‡] Floris J. van Eerden,[†] Alex H. de Vries,[†] and Siewert J. Marrink*,[†]

[†]Groningen Biomolecular Sciences and Biotechnology (GBB) Institute and Zernike Institute for Advanced Materials, University of Groningen, Nijenborgh 7, 9747 AG Groningen, The Netherlands

[‡]Faculty of Science, University of South Bohemia, Czech Republic, and Institute of Nanobiology and Structural Biology GCRC ASCR, v.v.i. Nove Hrady, Czech Republic

Supporting Information

ABSTRACT: We present an extension of the Martini coarse-grained force field to glycolipids. The glycolipids considered here are the glycoglycerolipids monogalactosyldiacylglycerol (MGDG), sulfoquinovosyldiacylglycerol (SQDG), digalactosyldiacylglycerol (DGDG), and phosphatidylinositol (PI) and its phosphorylated forms (PIP, PIP2), as well as the glycosphingolipids galactosylceramide (GCER) and monosialotetrahexosylganglioside (GM1). The parametrization follows the same philosophy as was used previously for lipids, proteins, and carbohydrates focusing on the reproduction of partitioning free energies of small compounds between polar and nonpolar solvents. Bonded parameters are optimized by comparison to lipid conformations sampled with an atomistic force field, in particular with respect to the representation of the most populated states around the glycosidic linkage. Simulations of coarse-grained glycolipid model membranes show good agreement with atomistic simulations as well as experimental data available, especially concerning structural properties such as electron densities, area per lipid, and membrane thickness. Our coarse-grained model opens the way to large scale simulations of biological processes in which glycolipids are important, including recognition, sorting, and clustering of both external and membrane bound proteins.

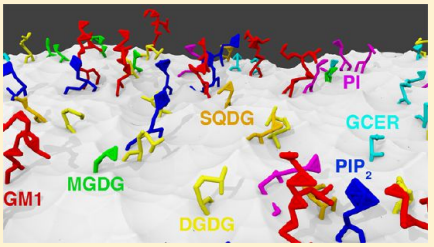

1. INTRODUCTION

Glycolipids are important components of the plasma membranes of most prokaryotic and eukaryotic cells and can be found in plants, bacteria, and mycoplasma as well as higher organisms. By virtue of their sugar residues and location on the cell surface, glycolipids can interact with a wide variety of small molecules and proteins that either reside in the aqueous phase or on the surface of neighboring cells.[1] Furthermore, they play an important role in lateral sorting and clustering of membrane embedded proteins.[2]

Glycolipids can be divided into two main classes: glycoglycerolipids and glycosphingolipids, which differ in the lipid backbone. The glycoglycerolipids consist of a glycerol backbone to which the sugar is attached. In the chloroplast and thylakoid membrane of plant cells, glycoglycerolipids are often the dominant class of lipids present, comprising as much as 50% of all lipid molecules in a cell.[3,4] Monogalactosyldiacylglycerol (MGDG) and digalactosyldiacylglycerol (DGDG) are the dominant glycoglycerolipids, usually accounting for 50% by weight of the total membrane lipids in higher plants. Another important glycoglycerolipid is phosphatidylinositol (PI) and its phosphorylated forms called phosphoinositides (PIPn). Inside the cell, the products of phosphoinositide metabolism are key membrane signaling molecules that play an important role in the regulation of membrane traffic, the cytoskeleton, nuclear events, and the permeability and transport functions of membranes.[5] Moreover, there is ample evidence that phosphoinositides present in membrane compartments are participating in biological membrane fusion and fission processes such as endocytosis and secretion.[5,6]

In glycosphingolipids, the sugar residue is linked with a glycosidic bond to the ceramide moiety of the sphingolipids. An important group of glycosphingolipids are cerebrosides, consisting of a ceramide with a sugar residue at the 1-hydroxyl moiety. The sugar residue can be either glucose or galactose; the two major types are therefore called glucocerebrosides (GluCer) and galactocerebrosides (GalCer). Cerebrosides are important components in animal muscle and nerve cell membranes. Gangliosides form another group of glycosphingolipids, with a headgroup consisting of oligosaccharides of galactose and glucose monomers, substituted with one or more sialic acids.

One of the particularly interesting membrane environments in which glycosphingolipids are commonly found are lipid rafts, that is, ordered functional nanoscale cell membrane domains that take part in various dynamic cellular processes such as membrane trafficking, signal transduction, and regulation of membrane proteins. In addition, glycosphingolipids can form domains known as glycosynapse, in contrast to the ones formed by cholesterol.[7] The presence of gangliosides at the plasma membrane makes them a target for a variety of bacterial toxins for initial recognition and infection of the host cell.[8]

Considering the importance of glycolipids, significant efforts have been made to understand their structure and dynamics in lipid bilayers. Biophysical methods such as nuclear magnetic resonance spectroscopy (NMR), X-ray diffraction, electron paramagnetic resonance spectroscopy (EPR), and fluorescence

Received: November 6, 2012
Published: January 16, 2013

dx.doi.org/10.1021/ct3009655 | J. Chem. Theory Comput. 2013, 9, 1694−1708

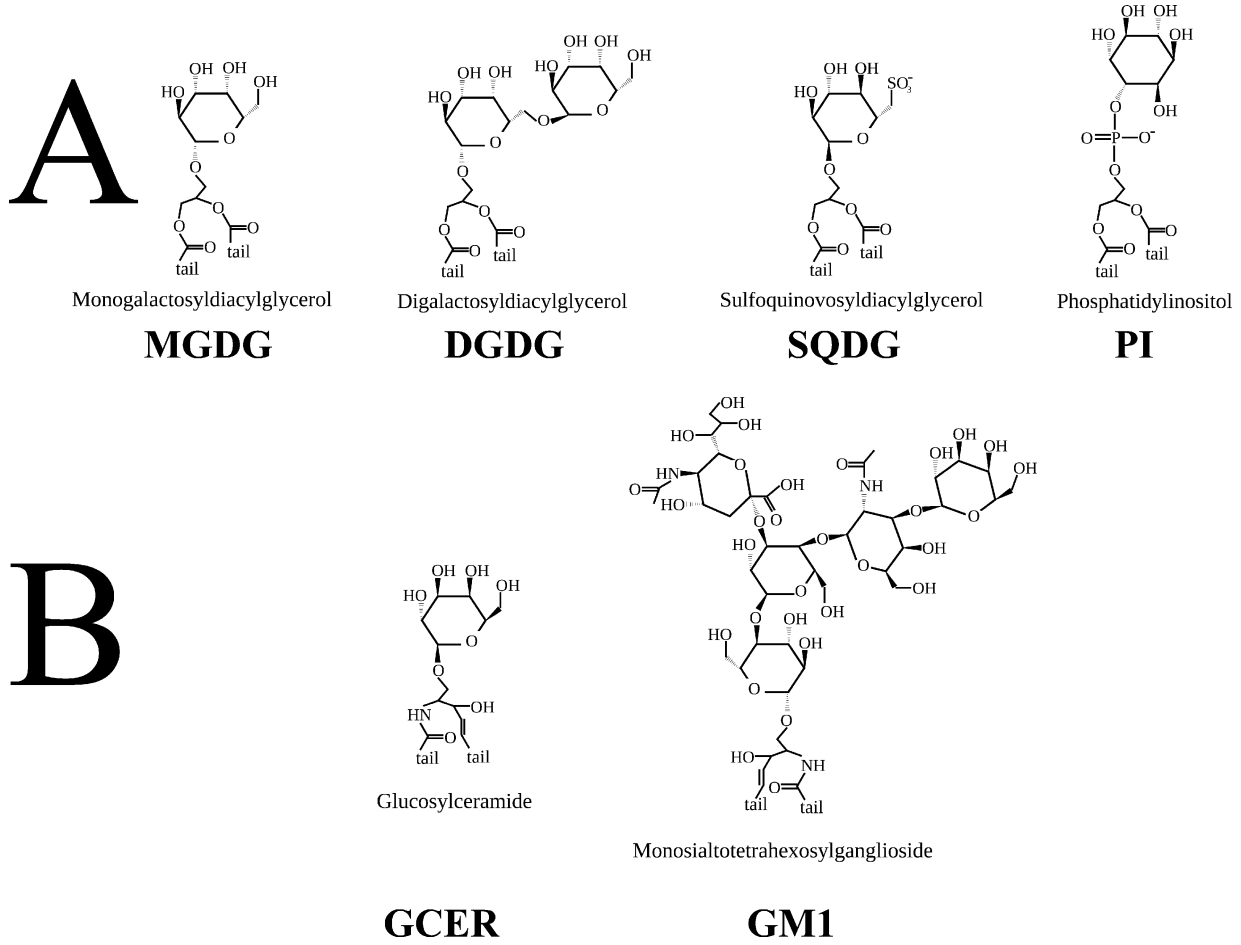

Figure 1. Atomistic representation of the glycolipids parametrized in this work. (A) glycerol linker based and (B) ceramide linker based.

spectroscopy have been used to understand the behavior of glycolipid membranes.[9−13] In general, it is found that both classes of glycolipids have the potential to modulate membrane physical properties. The high extent of hydroxylation of the head groups augments the capacity of these molecules to form hydrogen bonds, and hence the observed main phase transition temperature (Tm) of these molecules is much higher than expected compared to the corresponding glycerol or sphingosine based phospholipids. Due to large differences in Tm values, glycoglycerolipids and glycosphingolipids may segregate from phospholipids in membranes and form domains with high lateral packing density. The structure of the polar headgroup may, however, vary considerably from a single neutral monosaccharide to the large charged oligosaccharide in the case of gangliosides. A balance between the steric repulsion between the large head groups and attractive hydrogen bond interactions determines the detailed membrane behavior of these molecules. The acyl chain length and degree of saturation of glycolipids also play a major role in determining the glycolipid properties, but only a few biophysical studies address these points. Out of the several hundred glycoglycerolipids and glycosphingolipids found in biological membranes, thorough biophysical characterization has been carried out for a few glycolipids only, such as MGDG,[10] DGDG,[10] monoglycosylceramides,[14] lactosylceramides,[15] and gangliosides GM1 and GM3.[16] Data linking the structure and physical properties of glycolipids therefore is still fragmented and incomplete.

Molecular dynamics (MD) simulations can, in principle, provide the link between structure and physical properties. Simulations of lipid membranes have become standard and are used to study the interactions among many types of lipids and between lipids and proteins.[17] Simulation studies of glycolipids are also gaining more and more attention, for instance of pure MGDG and DGDG membranes,[18−20] certain PIPn,[21,22] GalCer,[13,23] and studies of bilayer systems containing various gangliosides.[24−32] However, these studies are performed at an all-atom (AA) level of resolution and are necessarily restricted to small system sizes of 100 000 to 1 million atoms and submicrosecond time scales. This suffices for simulation of small membrane patches (a few thousand lipids maximum) and observation of local packing effects but does not allow large scale simulation of glycolipid domain formation and reversible protein−glycolipid interaction, for instance.

An alternative to the AA approach is the use of coarse-grained (CG) force fields, which provide a useful methodology to study large systems on a long time scale at reasonable computational cost.[33] CG models can capture the most fundamental physical and chemical properties after averaging out some of the atomistic information, both spatially and temporally. A number of CGing approaches exist, either bottom-up in which the CG interactions are extracted from atomistic simulations or top-down in which experimental data are used to derive effective CG parameters. For a discussion on the advantages and disadvantages of these methods, the reader is referred to a number of recent reviews.[34−37] A popular force field for CG simulations of

dx.doi.org/10.1021/ct3009655 | J. Chem. Theory Comput. 2013, 9, 1694−1708

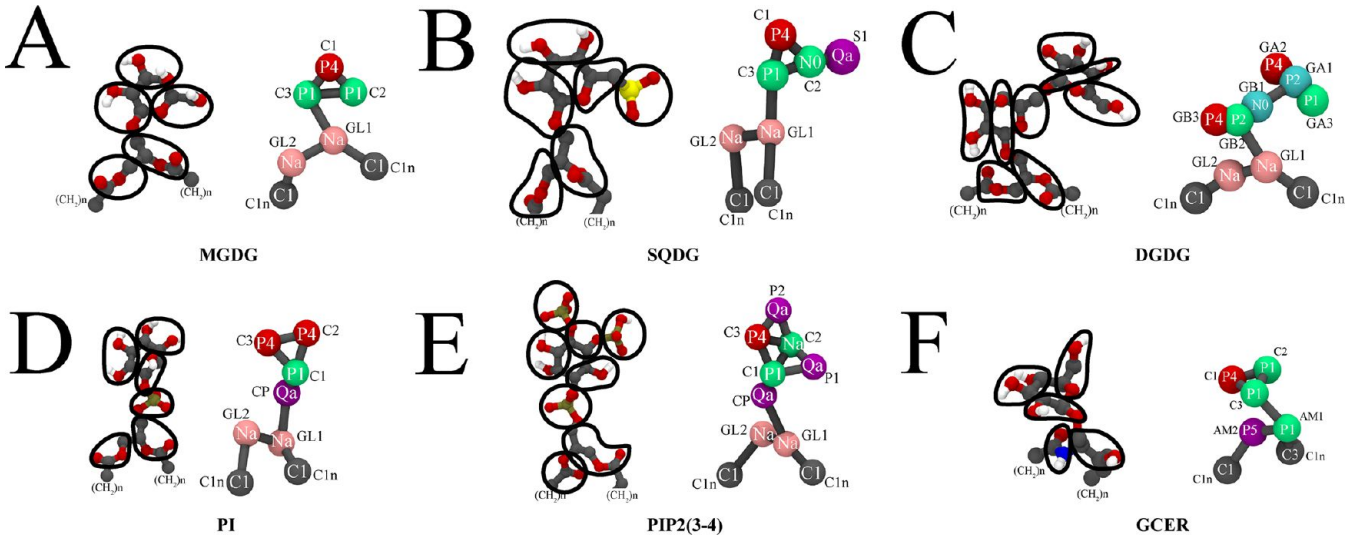

Figure 2. Mapping and CG bead assignment for MGDG (A), SQDG (B), DGDG (C), PI (D), PIP2(3, 4) (E), and GCER (F).

biomolecular systems has been developed in our group and coined the Martini force field.[38] It is based on a four-to-one mapping scheme, implying that on average four heavy atoms and associated hydrogens are represented as a single CG site. The Martini model has been parametrized extensively by using a chemical building block principle, incorporating both bottom-up and top-down information. Its key feature is the reproduction of thermodynamic data, especially the partitioning of the building blocks between polar and nonpolar phases. Recent additional testing of the Martini force field indicates a close agreement with all-atom and experimental data on, e.g., binding of pentapeptides to the membrane water interface[39] and dimerization of amino acid side chain analogues.[40] Developments up to date include the description of parameters for the simulation of lipids,[41] proteins,[42] and carbohydrates,[43] which makes it an excellent choice for the simulation of glycolipids.

In this work, we extend the Martini force field toward glycolipids. As the number of possible glycolipids is huge, we restrict ourselves to some of the biologically most relevant glycolipids, but the parametrization procedure can easily be extended to other glycolipids. The glycolipids that are parametrized are the glycoglycerolipids monogalactosyldiacylglycerol (MGDG), digalactosyldiacylglycerol (DGDG), sulfoquinovosyldiacylglycerol (SQDG), phosphatidylinositol (PI), the phosphoinositides PIP(3) and PIP2(3, 4), and the ceramide based lipids glucosylceramide (GCER) and monosialotetrahexosylganglioside (GM1). The structures of these lipids are shown in Figure 1. We set out with a description of the computational methods, including details of the CG model for each of the glycolipids considered. Then, we proceed with results pertaining to the comparison of conformational freedom of the CG lipids with respect to lipids modeled at the AA level. Finally, the behavior of the various glycolipid membranes is analyzed and compared with all atom and experimental data available.

2. COMPUTATIONAL METHODS

2.1. The Model. The Martini CG model is used for the basic parametrization of the glycolipid force field, which is therefore fully compatible with the Martini lipid,[38] protein,[42] and carbohydrate[43] models. In this section, we provide a brief overview of the basic parametrization procedure followed for glycolipids: definition of the mapping and parametrization of nonbonded and bonded interactions. Only the parametrization of the glycolipid head groups is described here; the tails of glycolipids do not differ from those of other lipid types and have been parametrized with the Martini model before.[38] More details about the basic Martini model can be found in the original articles.[38,42,43]

According to the mapping procedure for the Martini force field, on average four heavy particles are represented by one CG site. The glycolipid head groups consist of a mono-, di-, or oligosaccharide which can be adequately mapped on three beads per monomer as described previously.[43] Although this level of resolution preserves the geometrical shape of the sugar ring, distinction between different epimers (e.g., glucose, galactose, mannose) is lost.[43] Disaccharides are modeled as two three-bead units connected by a single bond, which mimics the glycosidic linkage. This geometry allows for the definition (and subsequent parametrization) of the glycosidic dihedral angles φ and ψ, which determine the relative orientation of the two sugar residues and the flexibility of the linkage. Likewise, the headgroup is connected to either the glycerol or sphingosine backbone of the glycolipid via a single bond. A number of additional angles and dihedrals is used to control the flexibility and orientation of the headgroup. An overview of the mapping of the main glycolipids considered in this work is given in Figure 2.

2.2. Parameterization of Nonbonded Interactions. Nonbonded interactions are described by a Lennard-Jones (LJ) 12−6 potential energy function:

$$U_{\mathrm{LJ}}(r) = 4\varepsilon_{ij}\left[\left(\frac{\sigma_{ij}}{r}\right)^{12} - \left(\frac{\sigma_{ij}}{r}\right)^{6}\right] \quad (1)$$

with σ_{ij} representing the distance at zero energy (collision diameter) between two particles i and j and ε_{ij} representing the strength of their interaction. The Martini model considers two different particle sizes: normal types and ring particle types, which differ in the σ_{ii} values of 0.47 and 0.43 nm, respectively. The ring-type particles are reserved for cases where the standard four-to-one mapping approach cannot be used, such as small ring-like molecules like benzene. The strength of the pairwise particle−particle interaction is determined by the value of the LJ parameter ε_{ij}. Larger values of ε_{ij} (i.e., stronger attraction) mimic polar interactions, whereas smaller values (weaker attraction) are

used to mimic the hydrophobic effect. In the full interaction matrix, four main types of interaction sites are differentiated: polar (P), nonpolar (N), apolar (C), and charged (Q). The special class of ring-type particles is further denoted by the prefix "S" and has a reduced value of ε_{ij}. Each particle type has a number of subtypes, which allows for a more accurate representation of the chemical nature of the underlying atomic structure. Within a main type, subtypes are either distinguished by a letter denoting the hydrogen-bonding capabilities, (d) donor, (a) acceptor, (da) both, or (0) none, or by a number indicating the degree of polarity (from 1, low polarity, to 5, high polarity). The Martini force field has been parametrized extensively to reproduce the correct partitioning free energies of small molecules (denoted building blocks) between a range of polar and apolar solvents. The full interaction matrix ε_{ij} can be found in the original publication.[38]

For the parametrization of novel compounds, the chemical nature of the underlying fine-grained structure is used to select the most appropriate building blocks and corresponding particle types. For saccharides, the most appropriate particle types are the class of "P" particles due to the polar nature of the sugar rings. The particle assignment for saccharides has been fine-tuned based on the partitioning free energy of monosaccharides and disaccharides between water and octanol, as described in ref 43. For the glycolipid head groups, initially the same particle assignment has been chosen as the corresponding saccharide. Some modifications of particle types proved necessary to reflect a modified polarity due to the link with the lipid backbone and to optimize some of the properties of the glycolipid membranes. Details of these modifications are described in the Results and Discussion section.

In addition to the LJ interaction, charged groups bearing a full charge q_i such as the sulfoquinovosyl and PI head groups, interact via a Coulombic potential energy function:

$$U_{el}(r) = \frac{q_i q_j}{4\pi\varepsilon_0\varepsilon_r r} \tag{2}$$

with relative dielectric constant ε_r = 15 or 2.5 for explicit screening in standard[38] or polarizable[44] Martini water, respectively. Note, in the current work, only the standard water model was used.

2.3. Parameterization of Bonded Interactions. Three types of bonded interactions are considered. CG particles chemically connected are described by a harmonic potential $V_{bond}(R)$:

$$V_{bond}(R) = \frac{1}{2}K_{bond}(R - R_{bond})^2 \tag{3}$$

where R_{bond} is the distance at which the potential is at a minimum and K_{bond} is the force constant of the bond. LJ interactions between bonded neighbors are excluded. Since the degrees of freedom are reduced at the coarse-grained level, it is necessary to preserve the rotameric states of different sugar−sugar and lipid−sugar linkages by using both angle and dihedral potentials. A cosine-based harmonic potential $V_{angle}(\theta)$ is used for the angles:

$$V_{angle}(\theta) = \frac{1}{2}K_{angle}[\cos(\theta) - \cos(\theta_0)]^2 \tag{4}$$

where K_{angle} and θ_0 are the force constant and equilibrium angle, respectively. For the dihedrals, a proper dihedral potential $V_{pd}(\phi)$ is used, with a multiplicity of 1:

$$V_{pd}(\phi) = K_{pd}[1 + \cos(\phi - \phi_{pd})] \tag{5}$$

In this case, ϕ denotes the angle between planes containing the beads *i,j,k* and *j,k,l*, with force constant K_{pd}.

The set of bonded parameters featured in eqs 3−5 has been parametrized by comparison to simulations of glycolipids at the AA level. To this end, the AA trajectories were converted to pseudo-CG trajectories using the center of mass of the appropriate fine grained particles.[45] The mapping between the AA and CG representation is shown in Figure 2. From the AA trajectory, the target distribution functions were obtained for the various bonds, angles, and dihedrals considered. In a couple of iterative steps, the CG parameters were adjusted manually to obtain the closest match between the pseudo-CG and real CG distributions.

2.4. Systems Simulated. For the parametrization stage, each type of glycolipid was simulated in two types of systems: a single glycolipid in aqueous solution and a pure glycolipid membrane. Both CG and AA simulations were performed in these setups. For the single glycolipid system, the lipid was placed in the center of a periodic cubic box with minimum wall-solute distances of 2 nm. A steepest descent algorithm[46] was used to relax the internal interactions in a vacuum. Subsequently, the box was filled with 2000 water molecules (AA) or 500 standard Martini water beads (CG), representing 2000 real water molecules, and the minimization procedure was repeated. The initial structures of all membranes were obtained by arranging the lipid molecules in a regular array in the bilayer (*x,y*) plane to obtain either 64 lipids per leaflet (AA) or 256 lipids per leaflet (CG). The membranes were then solvated with 5000 water molecules (AA) and 6000 water beads (CG), respectively. Before production time, the systems were pre-equilibrated by slow heating up to 310 K. To validate our models for the glycolipid head groups, additional simulations were performed of aqueous solutions containing the respective saccharides, both at the AA and CG level of resolution. To this end, eight sugars were placed in a cubic box and filled with water up to an 8 weight/weight (sugar/water) concentration.

In order to estimate the phase transition temperature of the different glycolipid membranes, we followed the protocol as explained in Marrink et al.[47] Pre-equilibrated CG or AA liquid-crystalline bilayer patches were cooled instantaneously to well below the main phase transition temperature of the glycolipid considered. From these quenching simulations, a configuration was selected in which part of the system was in the gel state and the other part was still fluid. This configuration served as the starting structure for subsequent simulations, exploring a temperature range around the anticipated transition temperature. For temperatures above the transition temperature, growing of the fluid domain is observed; for temperatures below the transition temperature, the gel domain expands. The phase transition temperature was thus pinpointed to a temperature window of ±5 K. All simulations were performed with the Gromacs simulation software version 4.0.[46]

2.5. Coarse-Grained Simulation Parameters. In the simulations at the CG level, we followed the standard simulation protocol used in the Martini parametrization.[38] The nonbonded interactions are cut off at a distance r_{cut} of 1.2 nm. To reduce the generation of unwanted noise, the standard shift function of Gromacs[46] is used in which both the energy and force smoothly vanish at the cutoff distance. The LJ and Coulomb potentials are shifted from r = 0.9 and r = 0.0 nm to the cutoff distance, respectively. The time step used to integrate the equations of

Table 1. Bonded Force Field Parameters for the CG Glycolipids Presented in This Work[a]

glycolipid	bonds[b]	R_{bond} nm	K_{bond} (kJ mol^{-1} nm^{-2})	angles	θ_0 (deg)	K_{angle} (kJ mol^{-1})	dihedrals	ϕ_{pd} (deg)	K_{pd} (kJ mol^{-1})
MGDG	C1−C2	0.3	30000	C1−C3−GL1	140.00	35	C1−C3−GL1−GL2	30.00	8
	C1−C3	0.3	30000	C2−C3−GL1	100.00	35			
	C3−C2	0.3	30000	C3−GL1−GL2	85.00	20			
	C3−GL1	0.426	30000	C3−GL1−C1A	131.00	25			
SQDG	S1−C2	0.262	30000	S1−C2−C1	150.00	20	C1−C3−GL1−GL2	30.00	8
	C1−C2	0.3	30000	S1−C2−C3	145.00	20			
	C1−C3	0.3	30000	C1−C3−GL1	140.00	35			
	C2−C3	0.3	30000	C2−C3−GL1	100.00	35			
	C3−GL1	0.426	30000	C3−GL1−C1A	85.00	20			
				C3−GL1−GL2	131.00	25			
DGDG	GA1−GA2	0.3	30000	GA2−GA1−GB1	81.00	35	GA2−GA1−GB1−GB2	−20.00	5
	GA1−GA3	0.3	30000	GA3−GA1−GB1	100.00	35	GB1−GB2−GL1−C1A	−80.00	5
	GA1−GB1	0.44	10000	GB2−GB1−GA1	180.00	35			
	GB1−GB2	0.3	30000	GB2−GL1−GL2	100.00	35			
	GB2−GB3	0.3	30000	GB3−GB2−GL1	106.00	35			
	GB2−GL1	0.5	10000	GB2−GL1−C1A	150.00	35			
PI	C1−C2	0.4	30000	C3−C1−CP	133.00	100	C3−C1−CP−GL1	−30.00	5
	C1−C3	0.4	30000	C2−C1−CP	100.00	70			
	C2−C3	0.4	30000	C1−CP−GL1	140.00	30			
	C1−CP	0.35	1250						
PIP(3)	C1−C2	0.4	30000	C3−C1−CP	133.00	100	C3−C1−CP−GL1	−30.00	5
	C1−C3	0.4	30000	C2−C1−CP	100.00	70			
	C2−C3	0.4	30000	C1−CP−GL1	140.00	30			
	C1−CP	0.35	1250						
	C2−P1	0.3	30000						
PIP(3,4)	C1−C2	0.4	30000	C1−CP−GL1	140.00	25	C3−C1−CP−GL1	−30.00	5
	C1−C3	0.4	30000						
	C2−C3	0.4	30000						
	C1−CP	0.35	1250						
	C2−P1	0.3	30000						
	C2−P2	0.35	30000						
	C1−P1	0.4	25000						
	C3−P2	0.31	30000						
	P1−P2	0.60	25000						
GCER	C1−C2	0.3	30000	C1−C3−AM1	50.00	200	C1−C3−AM1−AM2	125.00	10
	C1−C3	0.3	30000	C3−AM1−AM2	85.00	25			
	C2−C3	0.3	30000	C3−AM1−C1A	150.00	30			
	C3−AM1	0.57	20000	C1B−AM2−AM1	129.00	200			
	AM1−AM2	0.27	20000	AM1−C1A−C2A	180.00	25			
	AM1−C1A	0.37	20000	AM2−C1B−C2B	180.00	25			
GM1	GM1−GM2	0.37	30000	GM5−GM6−GM7	120.00	150	GM1−GM3−GM4−GM5	30.00	5
	GM2−GM3	0.31	20000	GM4−GM6−GM13	110.00	100	GM5−GM6−GM7−GM8	−130.00	5
	GM1−GM3	0.325	30000	GM7−GM6−GM13	110.00	25	GM4−GM6−GM13−GM14	−105.00	10
	GM3−GM4	0.35	30000	GM4−GM3−GM2	76.00	100	GM8−GM9−GM10−GM11	120.00	5
	GM4−GM5	0.39	30000	GM3−GM4−GM5	72.00	100	GM16−GM14−GM15−GM17	−105.00	15
	GM4−GM6	0.26	20000	GM6−GM7−GM8	71.00	50	GM1−GM3−GM4−GM6	0.0	5
	GM5−GM6	0.31	20000	GM7−GM9−GM10	70.00	100	GM5−GM6−GM7−GM9	−130.00	10
	GM6−GM7	0.35	20000	GM9−GM10−GM11	78.00	100	GM4−GM6−GM13−GM5	85.00	5
	GM6−GM13	0.34	20000	GM6−GM13−GM15	88.00	150	GM8−GM9−GM10−GM12	80.00	10
	GM7−GM8	0.505	20000	GM13−GM14−GM16	117.00	150	GM6−GM13−GM14−GM16	60.00	5
	GM7−GM9	0.34	30000	GM13−GM15−GM17	111.00	150	GM6−GM13−GM15−GM17	80.00	5
	GM8−GM9	0.31	30000	GM3−GM1−AM1	50.00	200	GM6−GM4−GM5−GM7	32.00	5
	GM9−GM10	0.36	30000	GM1−AM1−AM2	85.00	25	GM3−GM1−AM1−AM2	125.00	10

dx.doi.org/10.1021/ct3009655 | J. Chem. Theory Comput. 2013, 9, 1694−1708

Table 1. continued

glycolipid	bonds[b]	R_{bond} nm	K_{bond} (kJ mol^{-1} nm^{-2})	angles	θ_0 (deg)	K_{angle} (kJ mol^{-1})	dihedrals	ϕ_{pd} (deg)	K_{pd} (kJ mol^{-1})
	GM10−GM11	0.395	30000	GM1−AM1−C1A	150.00	30			
	GM10−GM12	0.265	30000	C1B−AM2−AM1	129.00	200			
	GM11−GM12	0.32	30000	AM1−C1A−C2A	180.00	25			
	GM13−GM14	0.34	30000	AM2−C1B−C2B	180.00	25			
	GM13−GM15	0.39	30000						
	GM14−GM15	0.36	30000						
	GM14−GM16	0.33	30000						
	GM15−GM17	0.3	30000						

[a]See Figure 2 for labeling nomenclature of the CG sites. [b]Bonds with force constants exceeding 25 000 are treated as a constraint in practice. An alternative parametrization of MGDG, DGDG, and SQDG can be found in the SI.

motion is 20 fs for most systems. Some glycolipids with more complicated structure were only stable with a reduced time step of 5 fs, however, as explained in the Results and Discussion section. Constant temperature is maintained by weak coupling of the solvent and solute separately to a Berendsen heat bath[48] with a relaxation time of 1 ps. Constant pressure is maintained at 1.0 bar by weak coupling to a pressure bath with a relaxation time of 1 ps. For the single glycolipid in solution as well as for the aqueous systems containing glycolipid head groups, this was done isotropically. For the bilayer systems, anisotropic coordinate scaling was performed. The box shape was fully flexible (triclinic) in order to allow for the development of hexagonal chain packing in the gel phase.

2.6. All Atom Simulation Parameters. The AA simulations of glycolipids were performed using a new glycolipid force field that is based on the GROMOS 53A6 force field parameters set[49] for the lipids and the GROMOS hexopyranose force field[50] for the head groups. Note that although the Gromos force field is a united-atom force field, we refer to it as AA. Details of this force field will be published separately; topologies are available upon request. The SPC water model[51] was used to model the solvent. In all cases, a 2 fs time step was used to integrate Newton's equations of motion. The LINCS algorithm[52] was applied to constrain all bond lengths with a relative geometric tolerance of 10^{-4}. Nonbonded interactions were handled using a twin-range cutoff[53] scheme. Within a short-range cutoff of 0.9 nm, the interactions were evaluated every time step based on a pair list recalculated every five time steps. The intermediate-range interactions up to a long-range cutoff radius of 1.4 nm were evaluated simultaneously with each pair list update and were assumed constant in between. To account for electrostatic interactions beyond the long-range cutoff radius, a reaction field approach[54] was used with a relative dielectric permittivity of 66. Constant temperature was maintained by weak coupling of the solvent and solute separately to a Berendsen heat bath[48] with a relaxation time of 0.1 ps. Pressure coupling was maintained at 1.0 bar using either isotropic coupling (sugar head groups and single glycolipid in solution) or through the anisotropic approach (bilayers), with a relaxation time of 1 ps. Mapping of the AA trajectories to pseudo-CG trajectories was performed at a frequency of once per 40 ps.

3. RESULTS AND DISCUSSION

3.1. Mapping and Parametrization. In this section, we explain the details of the mapping and parametrization of the glycolipids considered in this work. The parametrization is based partly on our recent extension of the Martini force field to carbohydrates[43] and partly on a thorough comparison of glycolipid conformations sampled at the CG and AA level of resolution. Note that the glycolipids were modeled with fully saturated palmitoyl tails, but other tails are easily substituted as the headgroup parameters are independent of the tail parameters. An overview of the mapping and parameters derived in this work is given in Figure 2 and Table 1. For the glycolipids MGDG, DGDG, and SQDG, we parametrized an additional model based on a slightly different mapping. This alternative model is slightly less accurate in reproducing AA data but is numerically more stable and therefore sustains a larger time step. Details and results for this alternative model are presented in the Supporting Information.

MGDG. The headgroup of MGDG consists of a galactose monomer which is directly linked to the glycerol backbone of a glycerolipid (Figure 2A). To parametrize the headgroup, we used the generic model for monosaccharides consisting of three hydrophilic particles connected by three bonds to represent the ring-like structure.[43] The choice of headgroup particle types follows the particle definition for glucose, which is an epimer of galactose and is indistinguishable at the resolution of the Martini model. Glucose consists of two "P4" particles, each representing part of the ring with two OH groups and a less polar "P1" particle to mimic the remaining part (Figure 2A). Due to the link with the glycerol unit, resulting in the loss of an OH group, the polarity of one of the "P4" beads is reduced to "P1" in case of MGDG.

Concerning the bond distances connecting the particles in the ring, at first we used the same parameters as for glucose.[43] However, these parameters required adjustment to improve the reproduction of the structural properties, especially the area per lipid (see next). The final bond length for each of the bonds in the MGDG headgroup is 0.3 nm, a decrease of 10−20% in comparison to glucose. The set of angle potentials describing the glycosidic linkage was parametrized in order to reproduce the most frequent states observed in AA simulations. We found that four angles were required, with θ_0 ranging from 80 to 140° and rather weak force constants. As can be observed in Figure 3, the

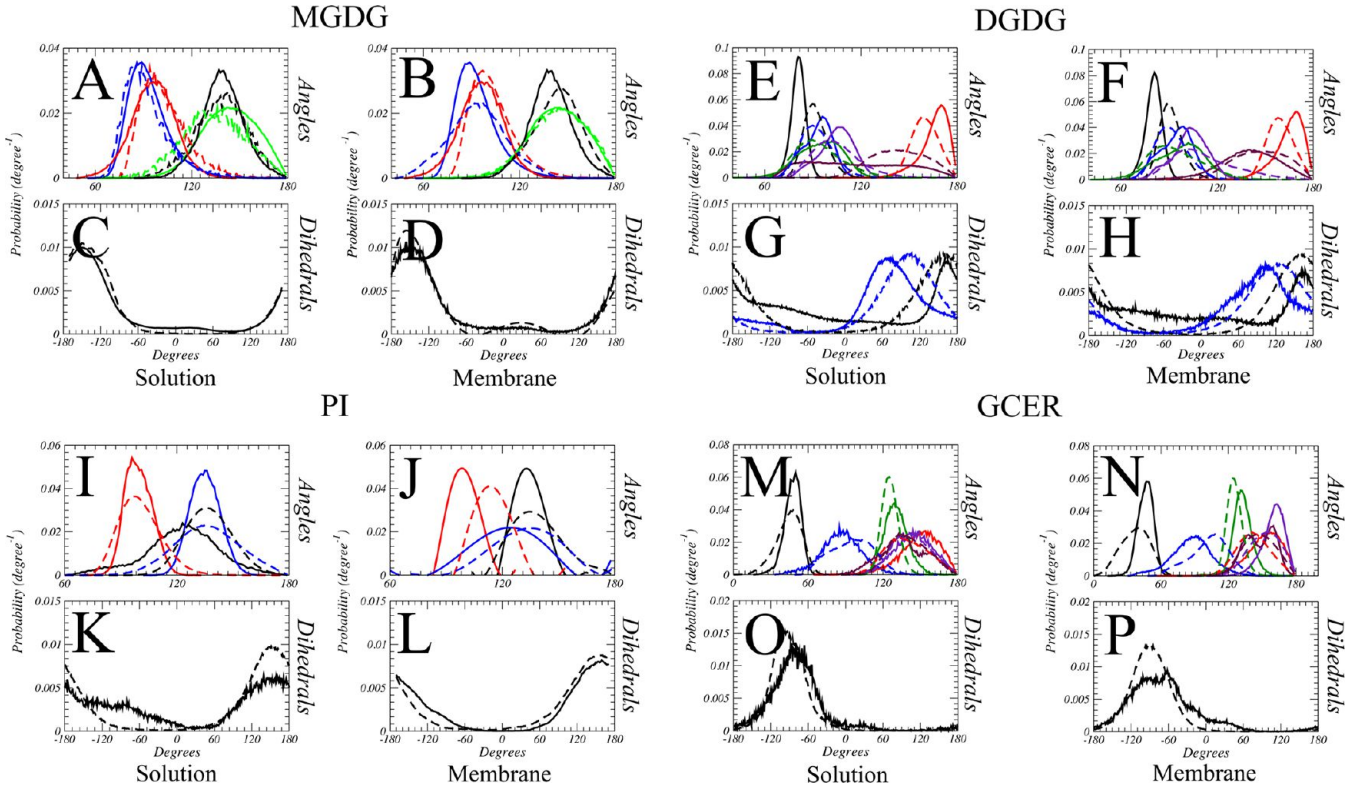

Figure 3. Angle and dihedral distributions for selected glycolipids. Angle (A, B, E, F, I, J, M, N) and dihedral (C, D, G, H, K, L, O, P) distributions were obtained through mapping the distributions from AA simulations (plain lines) and compared to the CG model (dotted lines). Both a single glycolipid in solution (A, C, E, G, I, K, M, O) and a glycolipid bilayer (B, D, F, H, J, L, N, P) were used as the reference state. Glycolipids compared are MGDG (A, B, C, D), DGDG (E, F, G, H), PI (I, J, K, L), and GCER (M,N,O,P). The definition of angles and dihedrals and respective colors are shown in Figure 4.

angle distributions are relatively unaffected by the system environment.

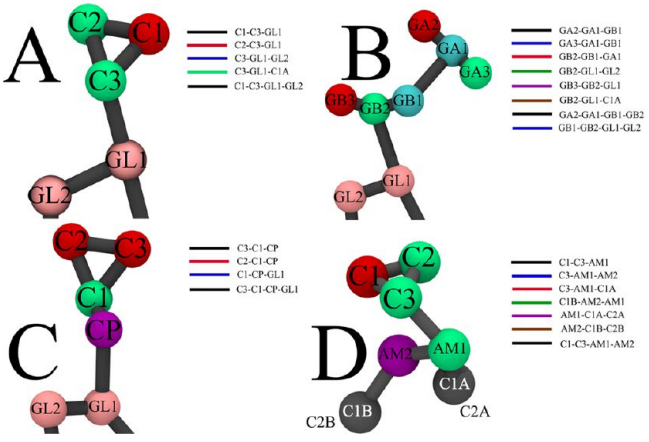

Figure 4. Definition of angle potentials for (A) MGDG, (B) DGDG, (C) PI, and (D) GCER. The color selection corresponds to the distributions shown in Figure 3.

Distributions obtained from the simulations of a single glycolipid in an aqueous environment (Figure 3A) are in good agreement with the ones obtained in a membrane (B) and easily reproduced by our CG model. The relative spatial orientation of the galactosidic ring was previously shown to be essentially unimodal through NMR and MD experiments.[55] The distribution can be represented by one dihedral consistent with our own AA data (Figure 3C and D). A drawback from the use of this dihedral is the necessity of a decrease of the time step from 20 (normally used for the simulation of proteins and carbohydrates) to 10 fs. The shorter time step prevents numerical instabilities arising from the geometric tension of the glycosidic linkage. An overview of all bonded parameters for MGDG can be found in Table 1. Notice that the parameters for the glycerol moiety are kept intact with respect to the standard lipid model.[38]

SQDG. The glycolipid SQDG is very similar to MGDG, however, with an additional sulfate group at carbon 6 of the galactose moiety. On the basis of the similarity, the SQDG topology follows the same mapping approach as MGDG. The sulfate group is represented by one bead of type "Qa," carrying a full negative charge. The subtype "a" is chosen to reflect the possibility of the sulfate group to act as a hydrogen bonding acceptor. The group is attached to the particle representing the hydroxymethyl group (cf. Figure 2B). The polarity decrease of the hydroxymethyl group due to the hydrolysis of one OH group is represented by the use of an intermediately polar "N0" bead. The close proximity between these two particles was best represented by a constraint, in order to avoid numerical instabilities. AA simulations (not shown) revealed that the relative orientation of the headgroup was the same as in the MGDG model, allowing us the use of the same bonded parameter set to mimic the orientation of the ring relative to the glycerol moiety.

DGDG. The headgroup of DGDG consists of a [α 1→6] linked digalactose unit. In the Martini model for carbohydrates,[43] disaccharides are modeled as two three-bead units connected by a single bond, which mimics the glycosidic linkage. This geometry allows for the definition (and subsequent parametrization) of the glycosidic dihedral angles which determine

dx.doi.org/10.1021/ct3009655 | J. Chem. Theory Comput. 2013, 9, 1694−1708

the relative orientation of the two sugar residues and the flexibility of the linkage. Thus, the mapping differs between a monosaccharide and the individual residues in a disaccharide. This somewhat nonobvious choice confers to the model the ability to represent the typical polar/apolar character of the disaccharides with the apolar region corresponding to the central part along the glycosidic linkage. The mapping and assignment of particle types of the first galactose ring in the DGDG headgroup follows that of maltose, which consists of two glucose monomers each represented by a "P4," "P2," and "P1" particle. The galactose linked to the glycerol moiety consists of a "P4," P2," and an "N0" particle and is mapped as illustrated in Figure 2C. To account for the loss of an OH group due to the glycosidic bond of the disaccharide, one of the beads was reduced in polarity to the level of an "N0" particle. The final topology for DGDG is shown in Figure 2C.

For the bonded interactions, we could not start from our previous parametrization of disaccharides as the [α 1→6] linkage was not considered. Atomistic simulations of single 1−6 bonded disaccharides in solution (e.g., isomaltose) have shown multiple rotameric states around the glycosidic bond,[56] which proved difficult to reproduce with the lower resolution of the Martini model. However, the dihedrals obtained after backmapping from our AA simulations of glycolipids, either of a single DGDG lipid in solution or a pure DGDG bilayer, show nearly a unimodal distribution. This distribution can be captured with our CG model, as is shown in Figure 3. The other bonded potentials are also unimodal and can easily be reproduced by the CG model (Figure 3). Three angular potentials are required to model the conformational flexibility of the disaccharide, plus three for the link to the glycerol backbone. Another dihedral is needed to control the relative orientation of the disaccharide with respect to the rest of the lipid. The parameters for the bonds are similar to those used for other disaccharides such as maltose.[43] An overview of all the parameters for DGDG is given in Table 1.

PI. Phosphatidylinositols are phospholipids with an inositol (cyclohexane-1,2,3,4,5,6-hexol) headgroup. Although inositol is not a classical sugar, PIs are usually classified as glycolipids. Due to the strong polarity of the inositol group, it was represented by three polar particle beads: two "P4" particles representing the di−OH units and one "P1" for the linker to the phosphate group (Figure 2D). Initially, the topology for the inositol headgroup started from the bonded parameters for the glucose ring. However, it turned out that these parameters result in an overstabilization of the gel phase of PI membranes, together with a too small area per lipid in the liquid phase. After several modifications, the equilibrium distance (R_{bond}) between the inositol particles was increased to 0.4 nm, which appeared to solve the problem (see below).

The relative position of the inositol group to the phosphate atom was described by three angles and one proper dihedral. A comparison of the distributions from the CG model to the backmapped atomistic data is shown in Figure 3. While in water every single angle is well represented, in the membrane the CG model falls somewhat short in reproducing the angle at 100° (red line). The full parameter set of PI is given in Table 1. Note that the parameters for the remainder of the lipid (phosphate and glycerol moieties) were kept identical to standard lipids in the Martini model.[38]

PIPn. The PIP headgroup consists of an inositol group which has been phosphorylated either once (PIP), twice (PIP2), or three times (PIP3) at the 3, 4, or 5 positions of the ring. In general, the inositol group from normal PI is used as a building block for the addition of different phosphate groups. As an example, the phosphate of PIP(3) can be easily represented by linking a "Qa" particle to the C2 CG bead of the inositol ring. Note that this CG bead carries a double negative charge, reflecting the charged state of the phosphate group. Due to the attachment of the phosphate group, resulting in the loss of an OH group, the polarity of the C2 particle should be decreased to "P1" type. The two particles are connected through a harmonic bond with an equilibrium distance of 0.3 nm and a K_{bond} of 30 000 kJ mol^{-1}, in practice replaced by a constraint. In the same way, the inositol headgroup can be modified in order to represent the PIP2(3,4). In this case, two additional CG particles are linked to the C2 site of PI. Each of these phosphates is modeled as a "Qa" particle and carries a doubly negative charge. Due to the double phosphorylation, the polarity of the C2 particle decreases even further and is now modeled by an "Na" bead. To ensure numerical stability of this model, which features a single site connected to four other CG particles, a number of auxiliary bonds are defined as listed in Table 1. Other PIP*n* lipids could be easily represented by making use of the same approach. Note that Martini models for PIP2(3,4) have been used in other studies recently;[57,58] however, these were rather ad hoc models that were not optimized with respect to AA simulations as is done here.

GCER. The glycosphingolipids glucosylceramide and galactosylceramide consist of a glucose and a galactose headgroup, respectively, linked to a sphingosine backbone. Within the resolution of the Martini model, we cannot distinguish between the two epimers glucose and galactose, so we present a single topology representative of both. Whereas the parameters for the monosaccharide headgroup can be taken from the glycoglycerolipid MGDG described above, the lipid sphingosine backbone has not yet been parametrized for Martini. To do so, we first considered ceramide (CER). Like the glycerol backbone of glycerolipids, the sphingosine backbone of CER is represented by two CG particles. The amide group is represented by a "P5" particle like the peptidic bond in proteins,[42] and the dihydroxyl group by a "P4" bead. The trans-bond connecting the dihydroxyl group with the rest of the aliphatic tail is represented by a "C3′" particle, as suggested for unsaturated bonds in the original model.[38]

Compared to glycerol, the bond between the two backbone beads needed a shorter distance and a higher force constant in order to reproduce the AA distance distributions. Whereas the bond between the glycerol backbone beads has an equilibrium distance of 0.37 nm and a force constant of 1250 kJ mol^{-1}, for the sphingosine backbone bond we obtained 0.27 nm and 30 000 kJ mol^{-1}. In practice this bond is replaced by a constraint. Three angle potentials were required to model the bending of the ceramide linkage properly (data not shown). Interestingly, the trans unsaturated bond of the sphingosine does not affect the alignment of the lipid tail very much in comparison to glycerolipids; at the CG level, it is represented by the same angle potential with θ_0 = 180° and K_{angle} = 25 kJ mol^{-1}.

On the basis of this model for CER, GCER is obtained by linking a galactose/glucose monomer to the AM1 bead, thereby reducing its polarity from a "P4" to a "P1" type. The sugar ring is represented by the same three particle beads and bonds as for the MGDG topology. The unimodal rotameric state of the ring is preserved through three additional angles and one dihedral, shown in Figure 2F. An overview of the bonded parameters for GCER is given in Table 1.

GM1. The glycosphingolipid GM1 is characterized by the presence of a branched oligosaccharide headgroup consisting of a

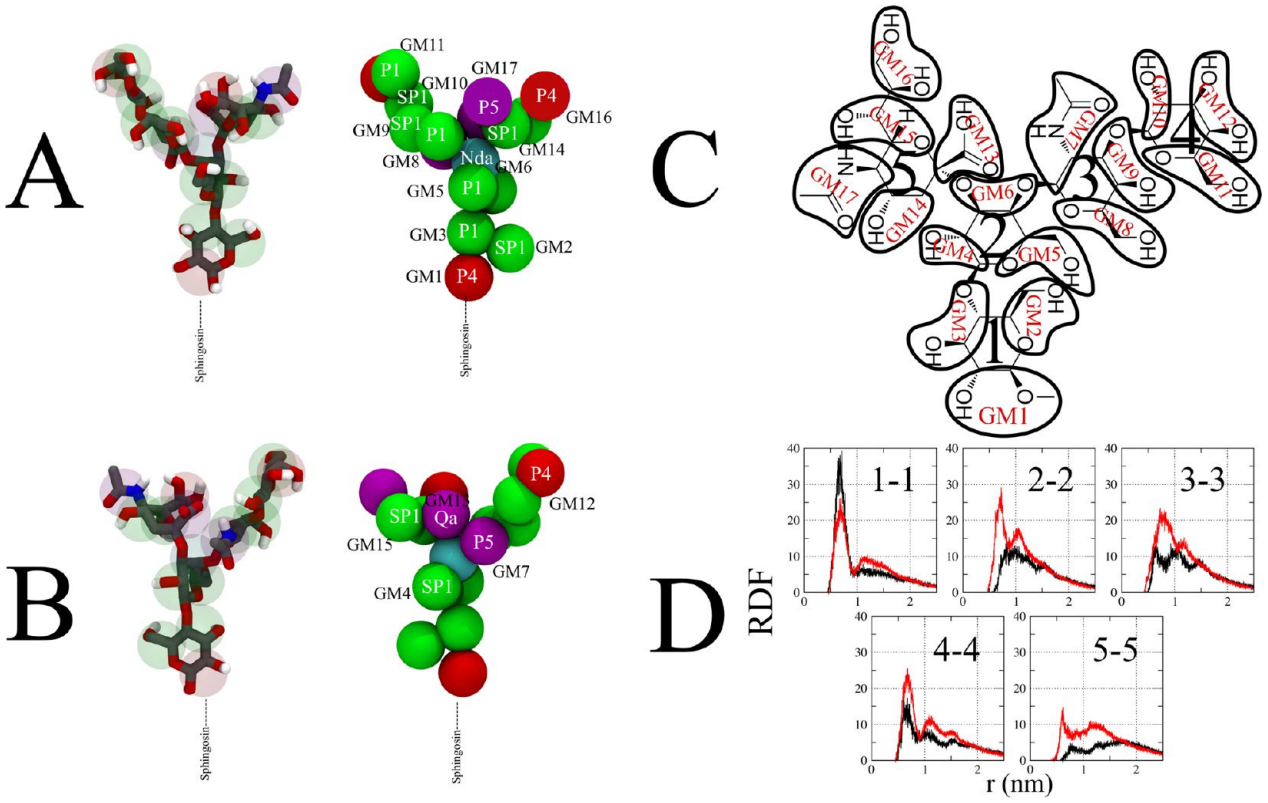

Figure 5. CG representation and mapping scheme of GM1. (A and B) The AA representation is shown to the left in ball and stick representation, with the mapping indicated by transparent spheres. The middle image shows the CG topology, with labels for the nomenclature and particle types of the CG beads. For clarification, two views of the molecule "front" (A) and "rear" (B) are given. (C) 2D representation of GM1 with indication of the mapping and numbering of rings for the RDF calculations. (D) RDFs of selected pairs of rings at both AA (black line) and CG (red line) resolution level. The full set of RDFs is presented as part of the Supporting Information.

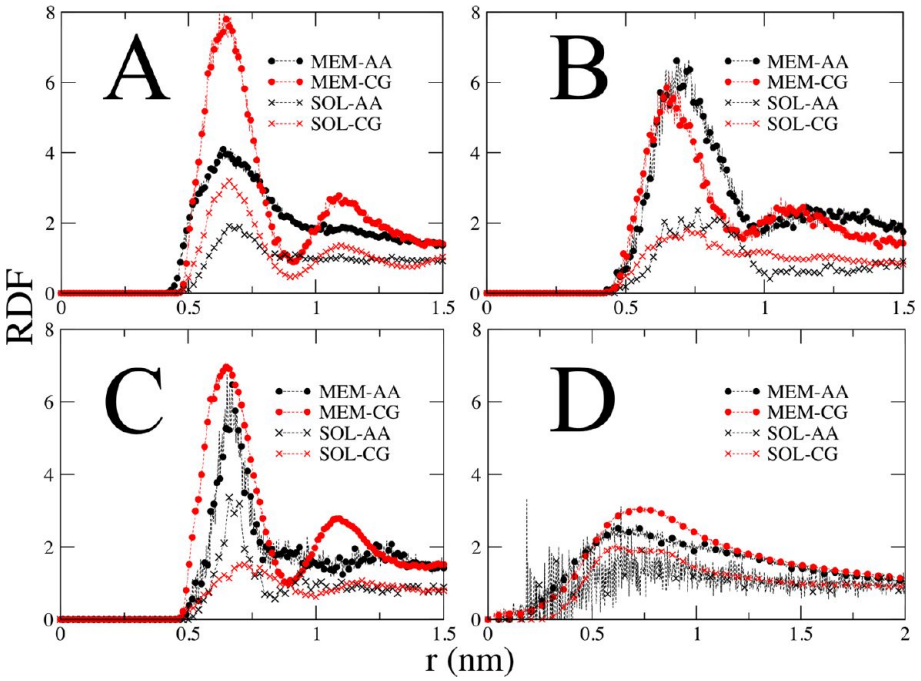

Figure 6. Radial function distributions (RDFs) of selected glycolipids. RDFs of the glycosidic head groups of pure MGDG (A), SQDG (B), PI (C), and DGDG (D) membranes, for both AA (black line) and CG (red line) resolution. RDFs were averaged either from sugar head groups in solution (crosses) or from membranes above the gel−liquid transition temperature (circles).

chain of glucose and galactosyl monosaccharides, as depicted in Figure 1B. These rings are consecutively connected through 1−4 and 1−3 glycosidic bonds. The glucose unit, in turn, is linked to a ceramide backbone. The second sugar monomer of the sugar

dx.doi.org/10.1021/ct3009655 | J. Chem. Theory Comput. 2013, 9, 1694−1708

Table 2. Selected Structural and Thermodynamic Properties for Common Glycolipid Membranes[a]

	area per lipid (nm^2)				membrane thickness (nm)						transition temperature (K)		
	gel		liquid		gel			liquid			gel–liquid		
glycolipid	CG	AA	CG	AA	CG	AA	exp	CG	AA	exp	CG	AA	exp
MGDG	0.51 ± 0.01	0.48	0.62 ± 0.01	0.63	5.0	4.8		4.0	3.9		325	~343	~343[†]
SQDG	0.49 ± 0.03	0.52	0.58 ± 0.07	0.57	5.0	4.5–5.12[b]		4.5	4.6	4.7[‡]	316	330	328[‡]
DGDG	0.56 ± 0.02	0.56	0.64 ± 0.01	0.67	4.4	4.2	4.5[‡]	4.1	4.2	4.5[‡]	300	320	315[‡]
PI	0.56 ± 0.02	0.53	0.62 ± 0.04	0.65	4.8	4–5[b]		4.0	3.9		298	320	320[§]
GCER	0.47 ± 0.01	0.44	0.56 ± 0.03	0.52	3.4–4.5[b]	3.9–5.0[b]	5.2[‖]	3.7	4	5[‖]	335	370	373[‖]

[a]Results are based on a 1 μs simulation for the CG model and 100 ns at the AA resolution. Area per lipid and membrane thickness were calculated 10 K below (gel) or above (liquid) the transition temperature of the membrane at the respective resolution. Error values in the structural properties were calculated from the variance between averages over individual blocks, using a block averaging procedure. Blocks were found to be statistically independent over 1–5 ns time intervals. The error in the membrane thickness is not explicitly shown, but less than 0.1 nm. The uncertainty in the transition temperature is about ±5 K for the CG model and ±10 K in the atomistic model. Experimental data were taken from (†) ref 62, (‡) ref 63, (§) ref 64, and (‖) ref 58. [b]Two peaks per interface are observed in the electron density profiles.

chain has a sialic acid residue (n-acetylneuraminic acid) linked to it, making the overall lipid anionic. Due to the high branching, we find that the most suitable CG representation is provided by the mapping approach used for monosaccharides, in particular glucose. For the CG particles representing a branching point, the polarity is reduced to "P1." In the second galactose ring, a double branching point is present, and the polarity of the respective CG particle is further reduced to the level of an "Nda" particle. The sialic acid group was represented by five particles, with the acetyl group represented by a "P4" particle, the carboxylic acid by "Qa" (carrying a negative charge), the glycerol unit as "P5," and the remaining parts of the sugar ring by two "P1" particles. For the final topology of the molecule, however, a number of normal beads were replaced by special ring particles. The distribution of these ring particles over the various monomers was optimized on the basis of a comparison between AA and CG simulations of solutions containing the GM1 oligosaccharide (see below). A closeup of the CG representation of GM1 is given in Figure 5A–C.

Optimization of the bonded interactions of the GM1 headgroup was again performed by comparison to distributions obtained from mapped AA simulations (data not shown). Consecutive CG beads are connected through a series of tight bonds with K_{bond} ranging from 20 000 to 30 000 kJ mol^{-1}. To match the conformations observed in AA simulations, a number of angle and dihedral potentials were used to control the flexibility and preferred orientation of the individual sugar ring units. However, the complicated conformation of the carbohydrate in combination with the tight force constants currently restricts the simulation time step to 5 fs.

Having most of the intra- and intermolecular features well represented, we settled on the CG topology given in Table 1. The rest of the GM1 molecule, i.e., the sphingosine backbone, is represented by the same particles used in the GCER model. Notice that the particle bead attached to the ceramide is replaced by a "P1" bead in its linked form.

3.2. Comparing Solutions of Glycolipid Head Groups at AA and CG Level. To validate and refine our topologies for glycolipids, we performed AA and CG simulations of aqueous solutions containing sugars mimicking the glycolipid head groups (see Computational Methods). To characterize the simulations, we calculated the radial distribution functions (RDFs) between the centers of mass of the sugars. The results are depicted in Figure 6 for MGDG, SQDG, PI, and DGDG at both AA (black line) and CG (red line) resolution. The CG data shown are based on the final topologies (Table 1). In the case of the monosaccharide head groups (MGDG, SQDG, and PI), the position of the first peak of the RDFs matches to within 0.05 nm, with a slight tendency toward too strong clustering at the CG level in the case of MGDG and an underestimation in the case of PI. The CG model further differs from the AA model by showing a more pronounced second peak, inherent of the ordering induced by the LJ 12–6 potential underlying the Martini model. In the case of the disaccharide headgroup of DGDG, no clear first peak is observed at the AA level. This feature is reproduced by the CG DGDG model. The low tendency for aggregation at both the AA and CG level is also evidenced through the RDFs of independent sugar rings (Figure S4C). For the oligosaccharides representative of the GM1 headgroup, RDFs were calculated between all five sugar rings, as shown in Figure 5D. In general, there is a reasonable agreement between the AA and the CG model in terms of radial structure, especially with respect to the position and magnitude of the first peak. The level of agreement between the two models proved very sensitive to the number and distribution of S-type particles in the CG topology, additional S-type beads leading to less aggregation and removal of them to the opposite behavior. The complete set of RDFs for all of the different ring–ring combinations of GM1 is provided in Figure S3.

3.3. Characterization of Glycolipid Membranes. In the next paragraphs, we give a detailed characterization of the properties of pure CG glycolipid membranes, focusing on a comparison to results from AA simulations and experimental data that were available. We found that many properties of the glycolipid bilayers can be reproduced on a semiquantitative level with the current set of parameters, including structural properties such as the area per headgroup and the density distributions across the membrane. Thermodynamic properties like phase transition temperatures are proving more problematic, however.

Structural Properties. On the basis of long simulations (1 μs) of small bilayer patches comprising 512 CG lipids, we calculated the area per lipid, the membrane thickness, the electron density profiles along the bilayer normal, and RDFs of the different glycolipid head groups. The area per lipid follows simply from the average lateral box dimensions divided by the number of lipids per leaflet, and the thickness is obtained from the peak–peak distance of the sugar head groups in the electron density profiles.

As a general trend, the CG model is able to reproduce the area per lipid both in the gel and in the liquid state in reasonably good agreement with reference AA simulations and experimental data available. Table 2 provides an overview of these structural properties for the main glycolipids studied. Agreement between

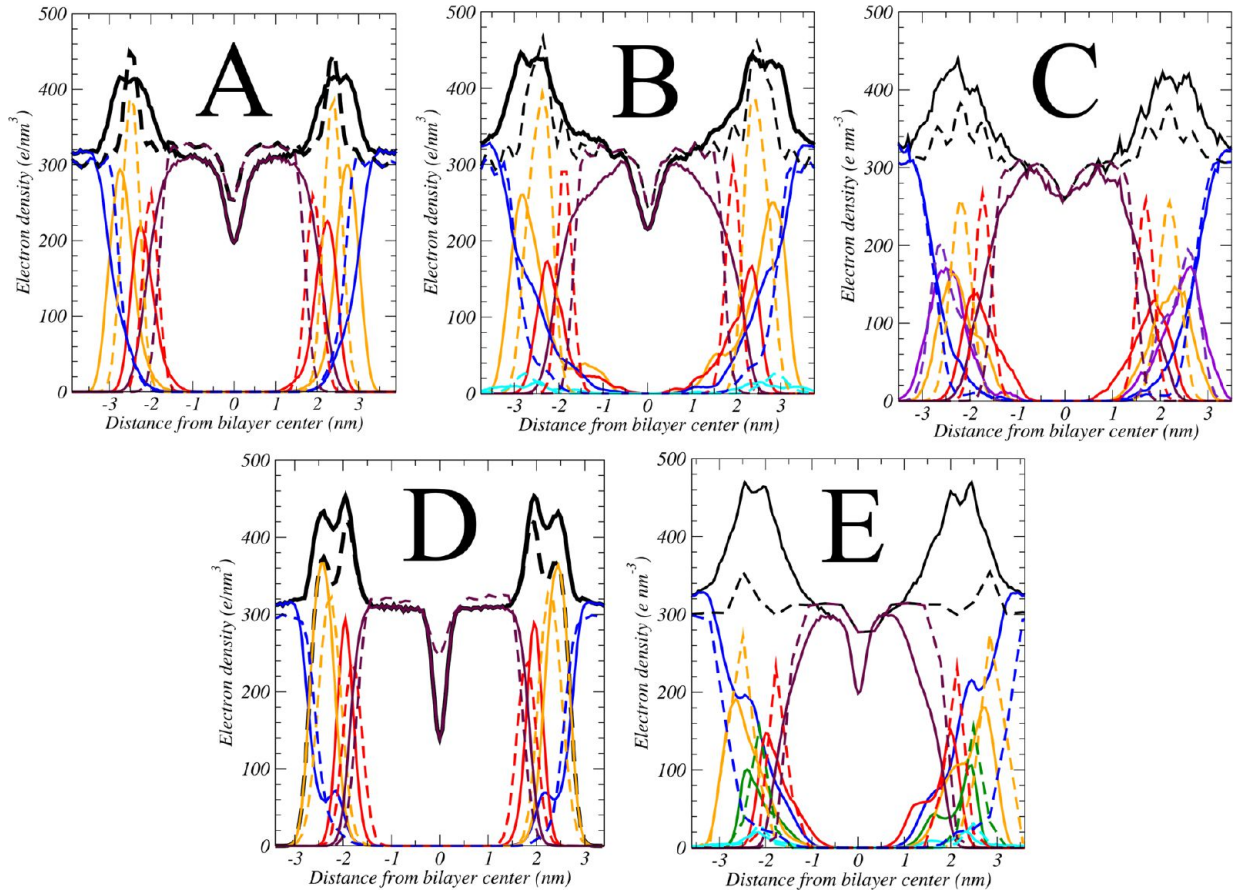

Figure 7. Electron densities of glycolipid membranes in the gel state. (A) MGDG, (B) SQDG, (C) DGDG, (D) GCER, (E) PI. Dotted lines are used for the CG model, solid lines for the AA level of resolution. Black lines, total electron density; orange, first sugar headgroup; magenta, second sugar headgroup if present; green, phosphate group; red, glycerol or ceramide linker; brown, aliphatic tails; blue, water; cyan, counterions.

CG and AA data is within 5%, either in the liquid and gel phase, which is comparable to the accuracy obtained for other lipids in the Martini model. The thickness of the CG bilayers also matches the atomistic value, to within 0.2 nm in most cases. Compared to the experimental data, the agreement is also good, though it should be kept in mind that experiments often rely on impure samples, making the direct comparison difficult.

To further characterize the structural properties of the glycolipid membrane, we calculated the electron density distributions for both the gel and fluid bilayers. Figure 7 compares the electron density profiles of the CG glycolipid bilayers in the gel state to profiles obtained from the atomistic simulations. The positions of the peaks in the electron density distributions coincide to within 0.2 nm for most of the membrane components. The CG model is even capable of reproducing some of the structural fine details, such as the presence of a double peak in the overall electron density profile of the headgroup region of GCER. In the liquid state (Figure 8), the electron densities also show a good agreement between both levels of resolution, with most peaks coinciding to within 0.2 nm. Some discrepancies remain, however, even after trying different topologies. For instance, in the case of PI, water is not able to penetrate the bilayer to the same depth in the CG simulations compared to the AA representation.

The intermolecular packing of the different glycolipid head groups was analyzed through a set of RDFs obtained from membranes in the fluid state. The results are depicted in Figure 6 for MGDG, SQDG, PI, and DGDG at both AA (black line) and CG (red line) resolution. The level of agreement is similar to that observed in aqueous solutions discussed above. Besides the somewhat overstructuring of the head groups at the CG level, the RDFs match reasonably well. Comparison of the independent sugar ring RDFs of DGDG (Figure S4) show overall good agreement. Moreover, the relatively increased ordering of the sugar rings (contrary to the structureless behavior in solution) observed at AA resolution is in general well reproduced by our CG model.

Taken together, we conclude that structurally, the CG model reflects most of the features found at the AA resolution at a semiquantitative level.

Thermodynamic Properties. Next to structural properties, the characterization of thermodynamic properties of the glycolipid membranes is important to judge the accuracy of our model. For all glycolipid membranes, we estimated the main phase transition temperature as explained in the Computational Methods section of this article. We also looked at phase behavior for specific glycolipids aiming at the reproduction of experimental behavior. In particular, we studied the formation of the inverted hexagonal phase for MGDG, the stability of micelles for GM1 lipids, and the formation of GM1 enriched domains in mixed lipid membranes.

The main phase transition temperatures, T_M, obtained for the glycolipid membranes are listed in Table 2. For the glycero-based glycolipids, T_M is underestimated by about 20 K as compared to AA membranes. The latter values are in good agreement with the experimental data.[59−61] The relative stability of the fluid phase

dx.doi.org/10.1021/ct3009655 | J. Chem. Theory Comput. 2013, 9, 1694−1708

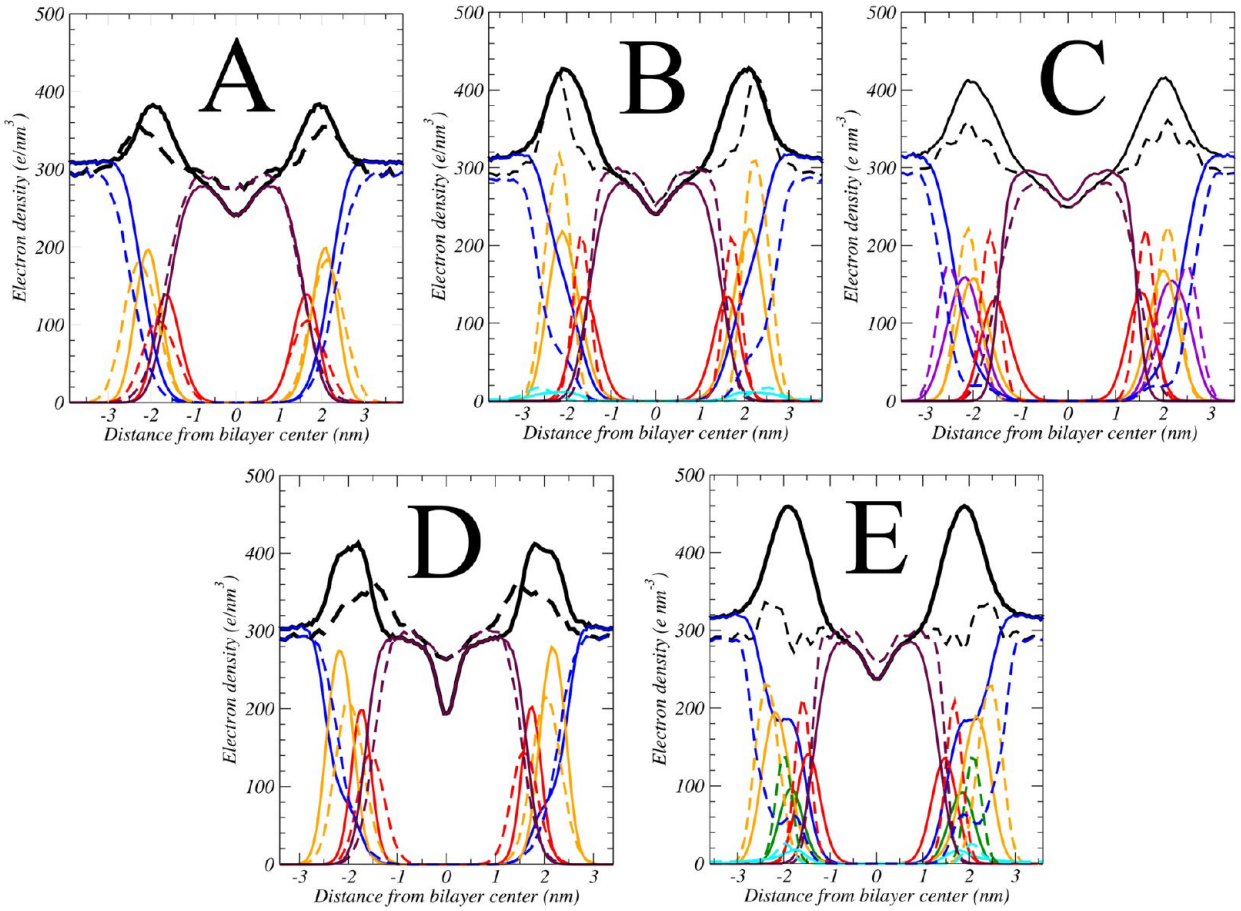

Figure 8. Electron densities of glycolipid membranes in the fluid state. (A) MGDG, (B) SQDG, (C) DGDG, (D) GCER, (E) PI. Dotted lines are used for the CG model, solid lines for the AA level of resolution. Black lines, total electron density; orange, first sugar headgroup; magenta, second sugar headgroup if present; green, phosphate group; red, glycerol or ceramide linker; brown, aliphatic tails; blue, water; cyan, counterions.

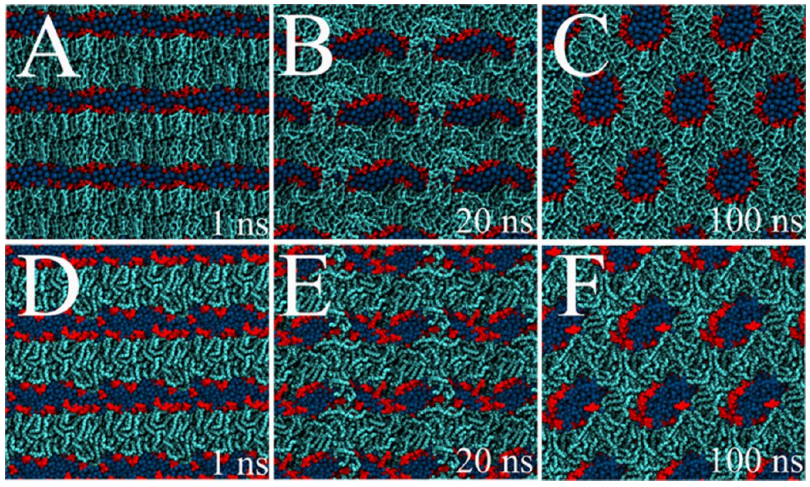

Figure 9. Transformation of a lamellar to an inverted hexagonal phase of 18−18:2 MGDG at 300 K. Snapshots taken from simulations at CG (A, B, and C) and AA (D, E, F) resolution. The system is viewed along the direction of the water channels. The simulations started from a lamellar conformation (A and D). Around 20 ns, stalks form connections between the lamellae (B and E) that eventually results in the formation of the H_{II} phase after 100 ns (C and F). The sugar groups are colored red, the glycerol backbone and tails cyan. Water is colored blue.

for these glycolipids is consistent with the behavior of other glycero-based lipids in the Martini model. For instance, the T_M of DPPC is also too low by about 20 K.[47] The origin of this discrepancy has been attributed to the CG nature of the lipid tails, which are unable to distinguish between, e.g., myristoyl and palmitoyl chains. The data in Table 2 pertain to lipids with palmitoyl tails; experimental transition temperatures for myristoylated lipids are typically about 20 K lower than their palmitoylated analogues. For the sphingo-based GCER lipid, however, the difference between the CG prediction and the AA model is almost 40 K, with the AA model again being close to the experimental value. The same is true for the CER membrane

dx.doi.org/10.1021/ct3009655 | J. Chem. Theory Comput. 2013, 9, 1694−1708

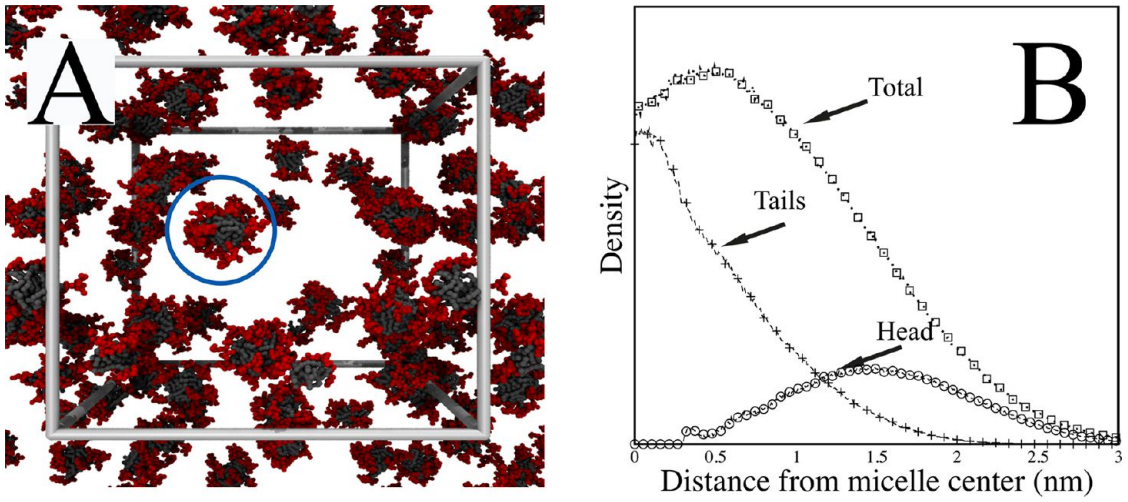

Figure 10. Distribution of coarse grained GM1 micelles after 3 μs of simulation. (A) The sugar groups are depicted red and the tails in dark gray. Water is not shown for clarity. The box edge length is shown in gray and measures 30 nm. (B) Radial density distribution of the micelle enclosed by a blue circle, showing the partial densities for the sugar headgroup and the aliphatic tails of GM1.

(results not shown), pointing to a potential problem with the sphingosine backbone. It has proven difficult to increase T_M for GCER without compromising the structural properties of GCER membranes, unfortunately. Given that the fluid phase is the biologically most relevant phase, we do expect the current model to be sufficient in most applications.

Although most natural glycolipids prefer the lamellar phase, unsaturation of one or two of the tails can trigger the formation of inverted phases. Whereas fully saturated MGDG prefers a lamellar geometry,[62] MGDG prefers an inverted hexagonal (H_{II}) phase for lipids containing one unsaturated aliphatic tail.[63] On the other hand, DGDG exhibits a bilayer structure under the same conditions. To study the phase preference of our CG model, two simulations were set up consisting of 128 MGDG lipids, initially in a lamellar conformation and solvated with 320 CG water molecules (16 real waters/lipid). The amount of water in the simulations is slightly below the maximum amount that can be taken up by the hexagonal phase of MGDG, which is about 20 waters per lipid according to experiments. In one of the simulations, one of the fully saturated tails of MGDG was replaced by a tail with double unsaturation, modeling 18−18:2 MGDG. The simulations were performed at a temperature of 300 K. In agreement with the experimental behavior, the fully saturated MGDG is stable in a lamellar (gel) phase, whereas the presence of an unsaturated tail results in the spontaneous formation of an inverted hexagonal phase. Simulations with different random starting conditions show the same behavior. Figure 9 shows a series of time frames of the phase transformation process. After 20 ns, the spontaneous formation of stalk-like connections between the lamellae is observed, which subsequently grow in the direction perpendicular to the projection plane. As a result, water channels are formed which line up in a hexagonal array, characteristic of the H_{II} phase. The whole process takes about 100 ns in total and is comparable to the transformation seen in DOPE bilayers.[41] For comparison, AA simulations were also set up under the same conditions and summarized in Figure 9. Both CG and AA resolution simulations depict basically the same process, and also within a similar time range.

Gangliosides, in contrast to the other glycolipids studied in this chapter, possess a branched oligosaccharide headgroup. The large size of this headgroup prevents most gangliosides from adapting stable lamellar phases by themselves. Instead, they form micelles in aqueous solution at concentrations above the critical micelle concentration (CMC).[64] For GM1, the CMC is 10^{-8} M.[65] Our parameters were tested against the experimental data by setting up a system composed of 50 GM1 molecules solvated by 250 000 CG water molecules. Thus, the concentration of the glycolipid is around 0.01 M, well above the CMC. After 3 μs simulation time, the GM1 indeed has formed small micelles, as can be clearly seen in Figure 10A. Although the micellar size distribution has not converged yet, the average micelle size is about 4−5 nm in diameter, in quite good agreement with the small-angle X-ray scattering (SAXS) and dynamic light scattering measurements reported by Orthaber et al.[64] The radial structure of one representative micelle is shown in Figure 10B, revealing a hydrophobic core extending to about 1−1.5 nm from the center, shielded from water by a broad layer of GM1 head groups.

Another interesting feature of the GM1 ganglioside is its ability to form small domains in model bilayers. In particular, AFM experiments[66] show that GM1 forms submicrometer-sized domains in a variety of PC and PC/cholesterol bilayers. These domains are on the order of 100 nm in diameter and have a 2 nm height difference with respect to the surrounding membrane. Also in raft-like PC/sphingomyelin/cholesterol mixtures, the presence of small GM1-rich domains was concluded from the same study.[66] To validate the capability of our parameters in reproducing this behavior, a bilayer system composed of DPPC and GM1 (10:1 molar ratio) was set up and simulated for 3 μs. Figure 11 shows the process of domain formation at the molecular level as revealed by our molecular dynamics simulations. Initially, the lipid components are randomized. Subsequent quenching of the mixture to 300 K (note: still above T_M for CG DPPC) leads to the rapid formation of a nanoscale GM1 domain. The size of the GM1 domain observed in our simulation is restricted by the number of GM1 lipids present in our system (48), but it was found to protrude 2 nm out from the bilayer consistent with the experimental AFM data.[66]

Overall, our glycolipid parameters are able to reproduce qualitatively the experimentally observed phase behavior, at least to the extent considered here. Precise pinpointing of the correct

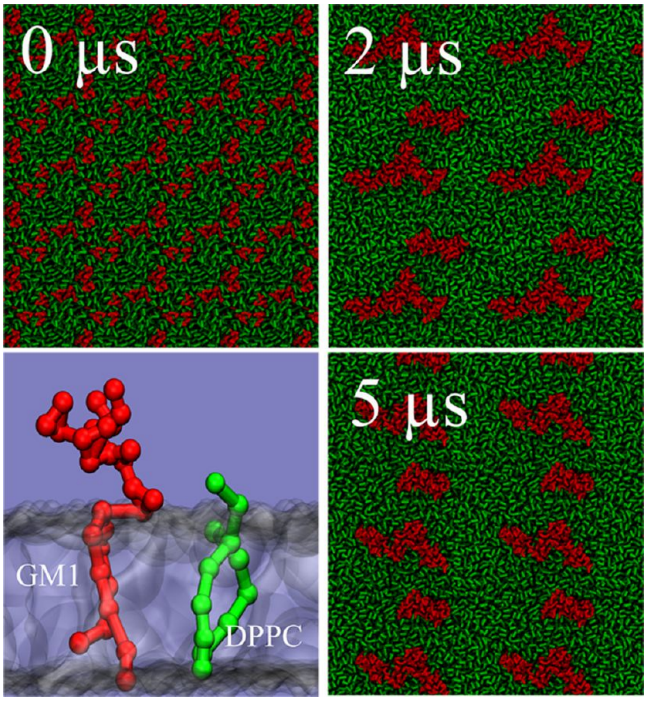

Figure 11. Spontaneous domain formation of GM1 in a DPPC bilayer, at 300 K. Bottom, left: Color coding of the lipid components. Green is used for DPPC, and red is used for the GM1 glycolipids. Other panels: Time-resolved phase segregation of the two-component membrane viewed from above, starting from a randomized mixture (0 μs), ending with a GM1 domain (3 μs).

transition temperatures remains inherently difficult for a CG model.

4. LIMITATIONS AND OUTLOOK

In this work, we present a set of parameters that allow simulations of glycolipids within the context of the Martini force field. Importantly, limitations of the model should be highlighted for optimal use. The model inherits certain limitations from the carbohydrate model[43] which are due to the limited resolution. For instance, different anomers and epimers in the hexopyranoses are represented by the same CG topology. Consequently, the topologies of galactose and glucose are indistinguishable, which carries over to our inability to differentiate between galactosyl and glucosylceramide lipids. Experimentally, these lipids show nearly the same structural characteristics,[67] which makes the requirement for distinction not so urgent. Another important simplification of the model is that puckering (i.e., *chair*−*chair* or *chair*−*boat* transformations) in the sugar rings is completely neglected. As in the carbohydrate model, only the chair $^4C_1$ state is represented. This does not pose a real problem, since most of the glycolipids present in membranes are mainly in the chair conformation.[68] Concerning the glycolipid bond connecting the sugar with the lipid, our atomistic simulations show that it exhibits primarily a single state which is easily represented using a dihedral potential at the CG level. However, the rotameric state of the two rings in DGDG is questionable. In solution, this sugar samples undoubtedly many states around the glycosidic bond. In a bilayer, the tight packing by neighboring lipids may restrict its conformation, but this could also be a kinetic effect that requires longer time scales than what can be assessed at the all-atom level. Evidence from NMR experiments and energy contour maps suggests that the interglycosidic bond may have three different rotameric states, albeit one is the most preferable.[69] A word of warning is also in place for our topology of GM1. The complicated conformational space of the oligosaccharide headgroup is not easily captured by a set of CG potentials. On longer time scales, and in processes where the GM1 headgroup interacts with other biomolecules (e.g., proteins), this might be a limiting factor. Finally, we want to stress that we only looked at a limited number of properties of the glycolipids considered in this work, mainly targeting the one component lipid membrane phase. Applications in mixed membranes, or in interactions with other molecules, should in general be considered with care.

Taken into account the limitations given above, the potential range of applications of the glycolipid Martini model in combination with the Martini parameters for lipids, proteins, and carbohydrates is very broad and promising. Application areas that we currently pursue include the specific interaction of membrane proteins with gangliosides and their putative role as raft shuttlers[70] and the structural and dynamical organization of the thylakoid membrane which is almost exclusively formed by the glycolipids MGDG, DGDG, and SQDG. In virtue of our parametrization approach, the model could be relatively easily extended toward many other different glycolipids, e.g., other members of the ganglioside family and lipopolysaccharides. Eventually our model could be used to represent the glycocalyx, the outer part of many cells.

In summary, a set of bonded and nonbonded parameters was extracted to model the dynamics and structure of a few biologically relevant glycolipids at the CG level. Standard particle types of the Martini force field were used, assuring that the model is fully compatible with other biomolecular components of this force field. Structural properties of the glycolipid systems such as the area per headgroup in the lamellar phase or the hexagonal spacing in the inverted hexagonal phase agree well with the AA and experimental data available. Compared to results obtained with atomistic simulations, atom density distributions are very similar in all cases considered. Thermodynamically speaking, the CG model has encouraging properties too. It not only provides a qualitatively correct propensity to form different phases, including lamellar, micellar, or hexagonal, but is also able to reproduce the phase separation for GM1/PC lipid mixtures in good agreement with experimental records. Given the underlying assumptions of our coarse-graining approach, our glycolipid model is another step in our aim toward a more realistic description of real cellular membranes.

■ ASSOCIATED CONTENT

Supporting Information

The alternative parameters for MGDG, SQDG, and DGDG as well as the complementary RDFs for DGDG and GM1 are provided. This material is available free of charge via the Internet at http://pubs.acs.org.

■ AUTHOR INFORMATION

Corresponding Author

*E-mail: s.j.marrink@rug.nl.

Notes

The authors declare no competing financial interest.

■ ACKNOWLEDGMENTS

Z.S. was supported by the HPC-EUROPA2 (project number: 228398) with support from European Commission Capacity

Area—Research Infrastructures Initiative, the Ministry of Education of the Czech Republic (ME09062, Aktion64p1), the Czech Science Foundation (grant 203/08/0114), and the University of South Bohemia (GAJU 170/2010/P).

REFERENCES

(1) Bush, C. A.; Martin-Pastor, M.; Imberty, A. *Annu. Rev. Biophys. Biomol. Struct.* **1999**, *28*, 269−293.
(2) Lingwood, D.; Simons, K. *Science* **2010**, *327*, 46−50.
(3) Gounaris, K.; Barber, J. *Trends Biochem. Sci.* **1983**, *8*, 378−381.
(4) Webb, M. S.; Green, B. R. *Biochim. Biophys. Acta, Bioenergetics* **1991**, *1060*, 133−158.
(5) Simons, K.; Gerl, M. J. *Nat. Rev. Mol. Cell Biol.* **2010**, *11*, 688−699.
(6) Mulet, X.; Templer, R. H.; Woscholski, R.; Ces, O. *Langmuir* **2008**, *24*, 8443−8447.
(7) Westerlund, B.; Slotte, J. P. *Biochim. Biophys. Acta, Biomembr.* **2009**, *1788*, 194−201.
(8) Connell, T. D. *Expert Rev. Vaccines* **2007**, *6*, 821−834.
(9) Hinz, H. J.; Kuttenreich, H.; Meyer, R.; Renner, M.; Fruend, R.; Koynova, R.; Boyanov, A.; Tenchov, B. *Biochemistry* **1991**, *30*, 5125−5138.
(10) Chen, J.-W.; Shi, K.; Zhang, L.; Huang, F. *Biochem. Biophys. Res. Commun.* **1992**, *186*, 1294−1298.
(11) Castro, V.; Dvinskikh, S. V.; Widmalm, G.; Sandstrom, D.; Maliniak, A. *Biochim. Biophys. Acta, Biomembr.* **2007**, *1768*, 2432−2437.
(12) Köberl, M.; Hinz, H. J.; Rapp, G. *Chem. Phys. Lipids* **1998**, *91*, 13−37.
(13) Zaraiskaya, T.; Jeffrey, K. R. *Biophys. J.* **2005**, *88*, 4017−4031.
(14) Barenholz, Y.; Bach, D.; Thompson, T. E.; Freire, E.; Correa-Freire, M.; Miller, L. R. *Thermochim. Acta* **1989**, *148*, 355−363.
(15) Slotte, J. P.; Oestman, A. L.; Kumar, E. R.; Bittman, R. *Biochemistry* **1993**, *32*, 7886−7892.
(16) Gupta, G.; Surolia, A. *FEBS Lett.* **2010**, *584*, 1634−1641.
(17) Marrink, S. J.; de Vries, A. H.; Tieleman, D. P. *Biochim. Biophys. Acta, Biomembr.* **2009**, *1788*, 149−168.
(18) Rog, T.; Vattulainen, I.; Karttunen, M. *Cell. Mol. Biol. Lett.* **2005**, *10*, 625−630.
(19) Róg, T.; Vattulainen, I.; Bunker, A.; Karttunen, M. J. *Phys. Chem. B* **2007**, *111*, 10146−10154.
(20) Kapla, J.; Stevensson, B.; Dahlberg, M.; Maliniak, A. *J. Phys. Chem. B* **2012**, *116*, 244−252.
(21) Lupyan, D.; Mezei, M.; Logothetis, D. E.; Osman, R. *Biophys. J.* **2010**, *98*, 240−247.
(22) Li, Z.; Venable, R. M.; Rogers, L. A.; Murray, D.; Pastor, R. W. *Biophys. J.* **2009**, *97*, 155−163.
(23) Hall, A.; Róg, T.; Vattulainen, I. *J. Phys. Chem. B* **2011**, *115*, 14424−14434.
(24) Roy, D.; Mukhopadhyay, C. J. *Biomol. Struct. Dyn.* **2002**, *19*, 1121−1132.
(25) DeMarco, M. L.; Woods, R. J.; Prestegard, J. H.; Tian, F. *J. Am. Chem. Soc.* **2010**, *132*, 1334−1338.
(26) Patel, R. Y.; Balaji, P. V. *J. Phys. Chem. B* **2008**, *112*, 3346−3356.
(27) Sega, M.; Jedlovszky, P.; Vallauri, R. *J. Mol. Liq.* **2006**, *129*, 86−91.
(28) Vasudevan, S. V.; Balaji, P. V. *J. Phys. Chem. B* **2001**, *105*, 7033−7041.
(29) Jedlovszky, P.; Sega, M.; Vallauri, R. *J. Phys. Chem. B* **2009**, *113*, 4876−4886.
(30) DeMarco, M. L.; Woods, R. J. *Glycobiology* **2009**, *19*, 344−355.
(31) Sega, M.; Vallauri, R.; Brocca, P.; Melchionna, S. *J. Phys. Chem. B* **2004**, *108*, 20322−20330.
(32) Mori, K.; Mahmood, M. I.; Neya, S.; Matsuzaki, K.; Hoshino, T. *J. Phys. Chem. B* **2012**, *116*, 5111−5121.
(33) Voth, G. A. In *Coarse-Graining of Condensed Phase and Biomolecular Systems*; CRC Press: Boca Raton, FL, 2008.
(34) Hyeon, C.; Thirumalai, D. *Nat Commun.* **2011**, *2*, 487−487.
(35) Lyubartsev, A. P.; Rabinovich, A. L. *Soft Matter* **2011**, *7*, 25−39.
(36) Bennun, S. V.; Hoopes, M. I.; Xing, C.; Faller, R. *Chem. Phys. Lipids* **2009**, *159*, 59−66.
(37) Deserno, M. *Macromol. Rapid Commun.* **2009**, *30*, 752−771.
(38) Marrink, S. J.; Risselada, H. J.; Yefimov, S.; Tieleman, D. P.; de Vries, A. H. *J. Phys. Chem. B* **2007**, *111*, 7812−7824.
(39) Singh, G.; Tieleman, D. P. *J. Chem. Theory Comput.* **2011**, *7*, 2316−2324.
(40) de Jong, D. H.; Periole, X.; Marrink, S. J. *J. Chem. Theory Comput.* **2012**, *8*, 1003−1014.
(41) Marrink, S. J.; de Vries, A. H.; Mark, A. E. *J. Phys. Chem. B* **2004**, *108*, 750−760.
(42) Monticelli, L.; Kandasamy, S. K.; Periole, X.; Larson, R. G.; Tieleman, D. P.; Marrink, S.-J. *J. Chem. Theory Comput.* **2008**, *4*, 819−834.
(43) López, C. A.; Rzepiela, A. J.; de Vries, A. H.; Dijkhuizen, L.; Hünenberger, P. H.; Marrink, S. J. *J. Chem. Theory Comput.* **2009**, *5*, 3195−3210.
(44) Yesylevskyy, S. O.; Schäfer, L. V.; Sengupta, D.; Marrink, S. J. *PLoS Comput. Biol.* **2010**, *6*, e1000810.
(45) Rzepiela, A. J.; Schafer, L. V.; Goga, N.; Risselada, H. J.; de Vries, A. H.; Marrink, S. J. *J. Comput. Chem.* **2009**, *31*, 1333−1343.
(46) Hess, B.; Kutzner, C.; van der Spoel, D.; Lindahl, E. *J. Chem. Theory Comput.* **2008**, *4*, 435−447.
(47) Marrink, S. J.; Risselada, J.; Mark, A. E. *Chem. Phys. Lipids* **2005**, *135*, 223−244.
(48) Berendsen, H. J. C.; Postma, J. P. M.; van Gunsteren, W. F.; Dinola, A.; Haak, J. R. *J. Chem. Phys.* **1984**, *81*, 3684−3690.
(49) Oostenbrink, C.; Villa, A.; Mark, A. E.; van Gunsteren, W. F. *J. Comput. Chem.* **2004**, *25*, 1656−1676.
(50) Lins, R. D.; Hünenberger, P. H. *J. Comput. Chem.* **2005**, *26*, 1400−1412.
(51) Berendsen, H. J. C.; Postma, J. P. M.; van Gunsteren, W. F.; Hermans, J. In *Interaction Models for Water in Relation to Protein Hydration*; Pullman, B., Ed.; Reidel: Dordrecht, The Netherlands, 1981; pp 331−342.
(52) Hess, B.; Bekker, H.; Berendsen, H. J. C.; Fraaije, J. *J. Comput. Chem.* **1997**, *18*, 1463−1472.
(53) van Gunsteren, W. F.; Berendsen, H. J. C. *Angew. Chem., Int. Ed.* **1990**, *29*, 992−1023.
(54) Tironi, I.; Sperb, R.; Smith, P.; van Gunsteren, W. F. *J. Chem. Phys.* **1995**, *102*, 5451−5459.
(55) Howard, K. P.; Prestegard, J. H. *J. Am. Chem. Soc.* **1995**, *117*, 5031−5040.
(56) Pereira, C. S.; Kony, D.; Baron, R.; Müller, M.; van Gunsteren, W. F.; Hünenberger, P. H. *Biophys. J.* **2006**, *90*, 4337−4344.
(57) Stansfeld, P. J.; Hopkinson, R.; Ashcroft, F. M.; Sansom, M. S. P. *Biochemistry* **2009**, *48*, 10926−10933.
(58) van den Bogaart, G.; Meyenberg, K.; Risselada, H. J.; Amin, H.; Willig, K. I.; Hubrich, B. E.; Dier, M.; Hell, S. W.; Grubmüller, H.; Diederichsen, U.; Jahn, R. *Nature* **2011**, *479*, 552−555.
(59) Lis, L. J.; Quinn, P. J. *Biochim. Biophys. Acta, Biomembr.* **1986**, *862*, 81−86.
(60) Graham Shipley, G.; Green, J. P.; Nichols, B. W. *Biochim. Biophys. Acta, Biomembr.* **1973**, *311*, 531−544.
(61) Redfern, D. A.; Gericke, A. *Biochem. J.* **2004**, *86*, 2980−2992.
(62) Mannock, D. A.; Brain, A. P. R.; Williams, W. P. *Biochim. Biophys. Acta, Biomembr.* **1985**, *817*, 289−298.
(63) Hato, M.; Minamikawa, H.; Tamada, K.; Baba, T.; Tanabe, Y. *Adv. Colloid Interface Sci.* **1999**, *80*, 233−270.
(64) Orthaber, D.; Glatter, O. *Chem. Phys. Lipids* **1998**, *92*, 53−62.
(65) Ohta, Y.; Yokoyama, S.; Sakai, H.; Abe, M. *Colloids Surf., B* **2004**, *33*, 191−197.
(66) Yuan, C.; Johnston, L. J. *Biophys. J.* **2001**, *81*, 1059−1069.
(67) Saxena, K.; Duclos, R. I.; Zimmermann, P.; Schmidt, R. R.; Shipley, G. G. *J. Lipid Res.* **1999**, *40*, 839−849.
(68) Shaw, N. *Bacteriol. Rev.* **1970**, *34*, 365−377.
(69) Howard, K. P.; Prestegard, J. H. *J. Am. Chem. Soc.* **1996**, *118*, 3345−3353.
(70) de Jong, D. H.; López, C. A.; Marrink, S. J. *Faraday Discuss.* **2013**, *161*, 347−363.